Numerical investigation of the DLR F15 two-element airfoil using a Reynolds stress model

Silvia Reuß[*], Axel Probst[†] and Tobias Knopp[‡]
Deutsches Zentrum für Luft- und Raumfahrt, Göttingen, Germany

Abstract

This work is dedicated to the appropriate representation of the experimental setup in the numerical prediction of the flow around multi-element airfoils. In the simulations a high-fidelity Reynolds-stress RANS-model is applied. The well established Menter-SST RANS-model is used as a reference. To assess the influence of the wind-tunnel walls three different numerical approaches with different computational complexity are compared: A three-dimensional simulation of the entire measurement section, a two-dimensional cut through the centerline of the test section and the same two-dimensional cut but with inviscid wind tunnel walls. The results show that it is sufficient to restrict the simulation to the centerline section of the wind tunnel and treat the wind-tunnel walls as inviscid walls.

Nomenclature

JHh	Jakirlic-Hanjalic-homogeneous
RSM	Reynolds-stress model
c	retracted chord length [m]
α	angle of attack [°]
C_l	non-dimensional lift-coefficient
μ_t	eddy viscosity [Pa·s]
k	turbulent kinetic energy [m^2/s^2]
d_w^+	wall distance in wall-units

1 Introduction

One of the most important goals in the numerical prediction of aerodynamical flows is to improve the prediction of the maximum lift for multi-element airfoils. Regarding the flow physics modeling, one major challenge is the correct prediction of the free shear-layers behind

[*]Research scientist, DLR, Bunsenstrasse 10, 37073 Göttingen, Germany, *silvia.reuss@dlr.de*
[†]Research scientist
[‡]Research scientist

upstream elements and their interaction with attached boundary layers on downstream elements under the influence of an adverse pressure gradient. The application of standard RANS-models does not yield always satisfying results for these test cases. Therefore, the high-fidelity JHh-v2 RSM [1] is used in this work. The mid term goal is to assess the possible advantages of hybrid RANS/LES simulations over pure RANS simulations. For a scale resolving simulation a very high resolution is needed. For this reason it is not feasible to model the entire experimental setup and it is desirable to restrict the numerical simulation to the centerline section. Therefore, it is important to investigate the differences between the experimental and numerical approaches. These investigations are performed using RANS simulations.

In this work three different approaches are compared: In the computationally most expensive approach the entire experimental section of measurements with resolved boundary layers on the wind tunnel walls as well as the three dimensional wind tunnel model is included in the simulation. In the second approach a two-dimensional cut through the centerline section of the wind tunnel is modeled and the influence of the side wall effects is neglected. In the third approach the upper and lower tunnel walls are treated as inviscid walls and the boundary layers at these walls are not resolved. This is the computationally least expensive and, therefore, the most desirable approach if scale resolving hybrid RANS/LES models are to be applied.

The investigated DLR F15 two-element airfoil is an industrially relevant test case in the framework of the *DFG Forschergruppe 1066 (FOR-1066)*. The experimental database for this test case is provided by other partners in the same project [2]. To reduce the wind tunnel side wall effects in the experimental setup, the model is equipped with droop noses at the model-wall junctions. The drooped leading edge of the main wing reduces the effective incidence angle and thus the separation at the model side wall junction.

2 Numerical method

The numerical simulations are performed with the DLR TAU code [3], a finite volume solver for the Navier-Stokes equations on unstructured meshes. The time-accurate simulations use a dual time-step scheme with an LUSGS solver. The spacial discretization uses central differences with artificial dissipation of matrix type. The turbulence equations are discretized using a second order Roe-scheme. The convergence is accelerated by a 3w multi-grid scheme. Different turbulence models are implemented for the closure of the Reynolds-averaged NS-equations.

In the present paper, the two-equation model Menter k-ω SST [4] and the JHh-v2 Reynolds-stress model [1] are applied. The latter is an extended and recalibrated variant of the JHh RSM [5] which applies a length-scale equation based on the homogenous dissipation rate ε^h as well as low-Reynolds damping functions to accurately model near-wall turbulence.

Grids. All grids were generated using the commercial grid-generation software Gridgen which provides the generation of structured as well as unstructured regions.

The desired strategy in the envisaged hybrid RANS/LES simulation is to regard only the centerline section of the experimental setup. This approach is chosen in the two-dimensional simulations. The first strategy is to use a cut through the centerline of the test section without resolving the boundary layers of the upper and lower wind tunnel walls and instead use Euler boundary conditions. For this approach two grids are compared. The first *grid 1* has a reasonable RANS resolution with about 84,000 points. About 60 hexahedral elements resolve the boundary layer in the wall normal direction with a first wall point at a distance of $d_w^+ \approx 1$ in wall-units. The main wing and flap are discretized with 430 and 240 points respectively.

A detail is shown in Fig. 1 (upper left). To check the grid influence, a second grid with a much finer resolution is used. This very highly resolved grid would be appropriate for a hybrid RANS/LES simulation. This *grid 2* has about 200,000 points in the x-z plane. About 100 hexahedral elements resolve the boundary layers in the wall normal direction. The first node above the wall is located at a distance of about $d_w^+ \approx 0.4$ in wall-units. The surface of the main wing element is discretized with 685 points and 480 points are located on the surface of flap.

In the second approach the effects of the upper and lower wind tunnel walls are taken into account. *Grid 1* was modified to resolve the boundary layers at these walls with about 60 hexahedral cells. The grid is shown in 1 (lower left).

The three-dimensional grid is based on the modified *grid 1* as the centerline section. The surface grid is shown in Fig. 1 (right). The grid encloses one half of the experimental setup and uses a symmetry boundary condition at the centerline section. It contains 7.5 million grid points.

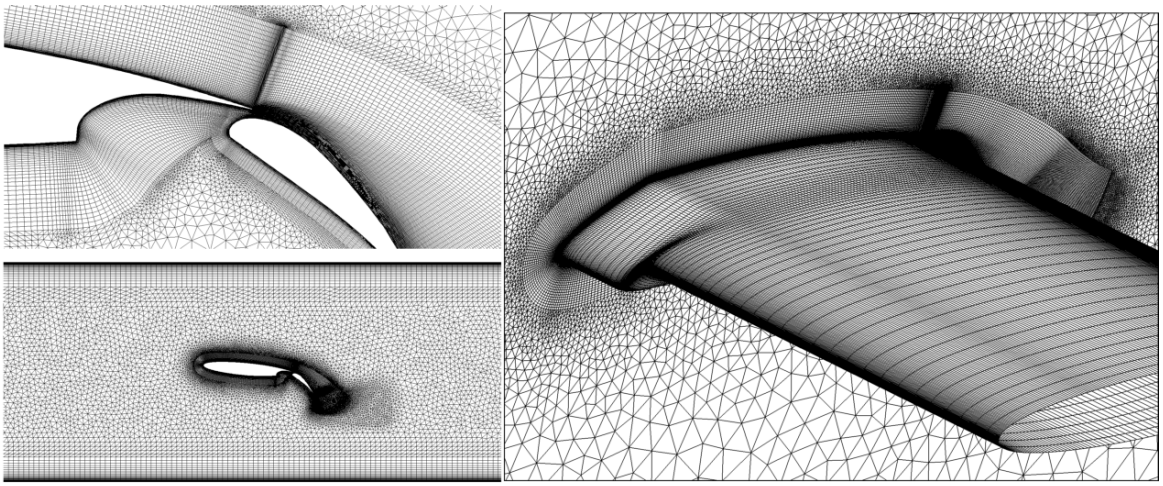

Figure 1: Two- and three-dimensional grids used in the presented simulations

3 Test case description

The experimental setup consists of the measurement section of the wind tunnel and the measured F15 two-element profile. The wind tunnel has a quadratic inlet section with an edge length of 1.3m. The entire test section has a length of 7.55m. Over a length of 5.7m the upper and lower wall diverge. Over the last 1.85m the upper and lower wall are retracted again. In this last section the side walls are also retracted. The profile has a retracted chord length of $c = 0.6$m. The span-wise extend of the wind tunnel model is 1.3m. The model is positioned 3.9m behind the inlet section at a centered position. The flap is deployed with a deflection angle of $\alpha_{flap} = 35°$. Detailed experimental data including static pressure measurements at the centerline section of the model and the upper and lower wall of the wind tunnel, PIV data and oil-flow pictures were taken at incidence angles of $\alpha = 0°$ and $\alpha = 6°$. These two incidence angles are used in the following simulations. The measurements were performed with a velocity of 50m/s at a Reynolds number of about 2 million and a Mach number of about 0.15.

4 Results

In this section the results that were obtained with the different strategies described above are compared. In the first subsection the computationally least expensive results that were obtained using a two-dimensional cut in the centerline section and inviscid boundary conditions for the upper and lower wind tunnel wall are compared. This relatively inexpensive approach is used to investigate the influence of the grid resolution and the time-step size. Also a principal difference between the solutions of the two applied turbulence models, the Menter-SST and the JHh-v2 RSM model, is observed. The reason for this difference is investigated. In the next subsection the results that were obtained in the simulations that take into account the wind tunnel walls are presented and compared to the previously described results and to the experimental data.

4.1 2D simulations with inviscid upper and lower wind tunnel wall

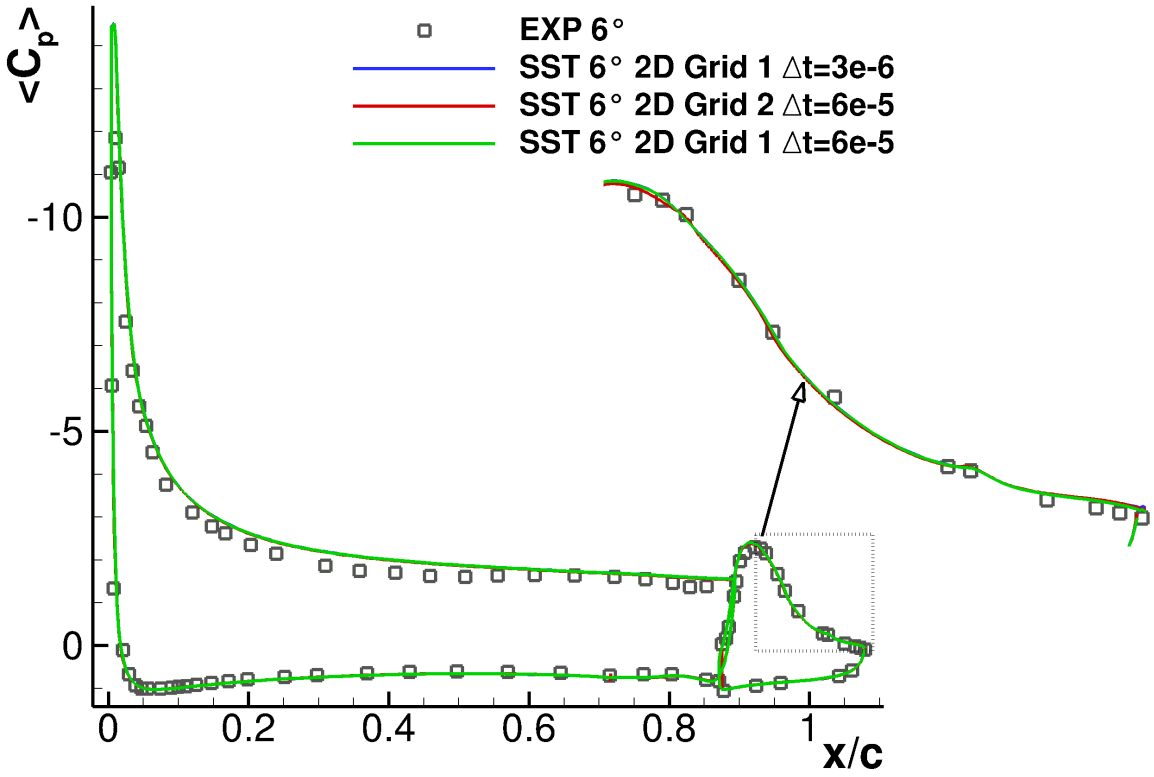

Figure 2: Pressure distribution with Menter-SST model on *grid 1* with different time steps and on *grid 2*

First the appropriate mesh resolution and time-step size are investigated. In Fig. 2 three time-accurate simulations using the Menter-SST model at an incidence angle of $\alpha = 6°$ are compared. The mean-pressure distribution, averaged in time, obtained with different grids and time-steps are shown. The green line is the pressure distribution on the coarser *grid 1* while the red line is computed on the finer *grid 2*. There is hardly any difference between the two results and thus it is justified to use the coarser grid in the following simulations. The influence of the time-step can be seen in the comparison of the green line and the blue line. In the former simulation a physical time-step of $\Delta t = 6 \cdot 10^{-5}$s is used. This corresponds to 200 time-steps per convective time unit. The blue line is from a simulation with a physical time-step of

$\Delta t = 3 \cdot 10^{-5}$s, corresponding to 400 time-steps per convective time unit. The only difference between these two lines can be seen at the very rear end of the flap in the zoomed perspective. This difference is due to the resolution of the instabilities that form behind the blunt trailing edge of the flap and has no influence on the overall flow. Thus it is justified to use a time-step of $\Delta t = 3 \cdot 10^{-5}$s in the following simulations.

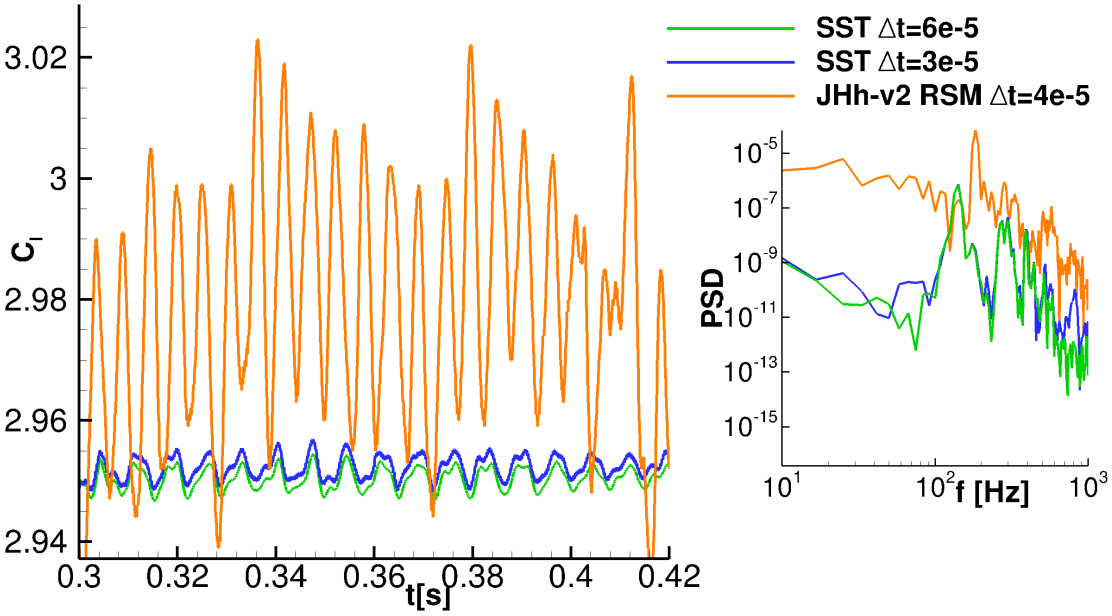

Figure 3: Time curve of the lift-coefficient from Menter-SST and JHh-v2 RSM simulations and corresponding sound-pressure-level

This finding is confirmed by the time curve of the lift-coefficient that is shown in Fig. 3. The green and blue lines are the results discussed earlier. The main behavior is the same in both simulations. There is a very small difference of the mean lift that is $C_l = 2.95$ with a time-step of $\Delta t = 6 \cdot 10^{-5}$s and $C_l = 2.952$ with a time-step of $\Delta t = 3 \cdot 10^{-5}$s. This little difference is again due to small differences in the very rear part of the flap and can be neglected. The distinct peak in the sound-pressure-level at a frequency of 144 Hz shows up in both simulations. With the smaller time-step the level of the larger frequencies is higher. The orange line in Fig. 3 is from a JHh-v2 RSM simulation on the coarser grid. Here the lift-curve oscillates with comparatively high amplitudes with a peak frequency of 185 Hz and the mean lift is $C_l = 2.979$.

The time-accurate Menter-SST simulations converge to a nearly steady state. This is not the case for the JHh-v2 RSM model. The flow in the cove of the main wing is highly unsteady. The instantaneous streamlines in the cove at two different instances in time are shown in Fig. 4. The separation bubble blows up and then breaks down again, splitting into two smaller bubbles.

The reason for this instability is shown in Fig. 5. Here the ratio of the modeled turbulent eddy-viscosity to the laminar eddy-viscosity is shown. In the RSM simulation the modeled turbulent eddy-viscosity is computed as $\mu_t = 0.09 \cdot \rho \cdot k_{RSM}^2/\varepsilon$, with $k_{RSM} = 0.5 \cdot R_{ii}$ with the normal Reynolds-stresses R_{ii}. The level of modeled turbulence in the wing cove is considerably smaller in the JHh-v2 RSM simulation. Here the $\alpha = 0°$ case is shown but the same observation can be made for $\alpha = 6°$.

This low level of modeled turbulence in the RSM simulation is due to a very quick decay of

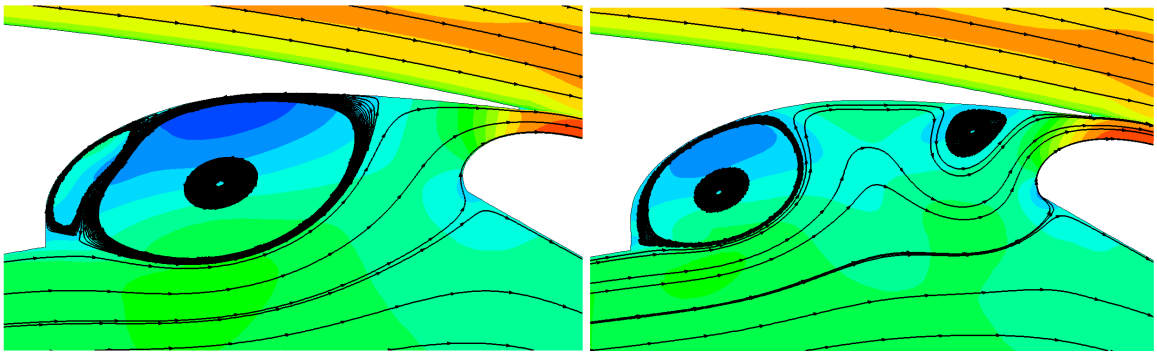

Figure 4: Instantaneous streamlines in the wing cove at $\alpha = 0°$ predicted with the JHh-v2 RSM model

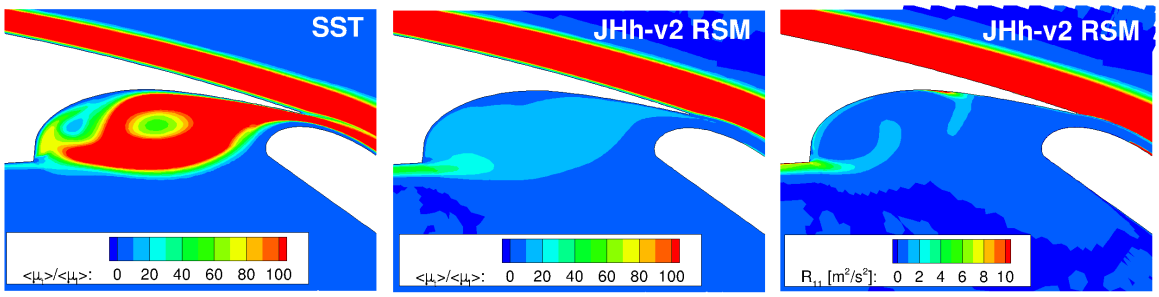

Figure 5: Eddy-viscosity of the Menter-SST (left) and the JHh-v2 RSM simulation (middle) and Reynolds-stress R_{11} (right)

the modeled Reynolds-stresses right behind the geometry-fixed separation point at the sharp edge. The distribution of the first normal component of the Reynolds-stress tensor is shown on the right in Fig. 5. The same rapid decay of modeled Reynolds-stress occurs for all other components.

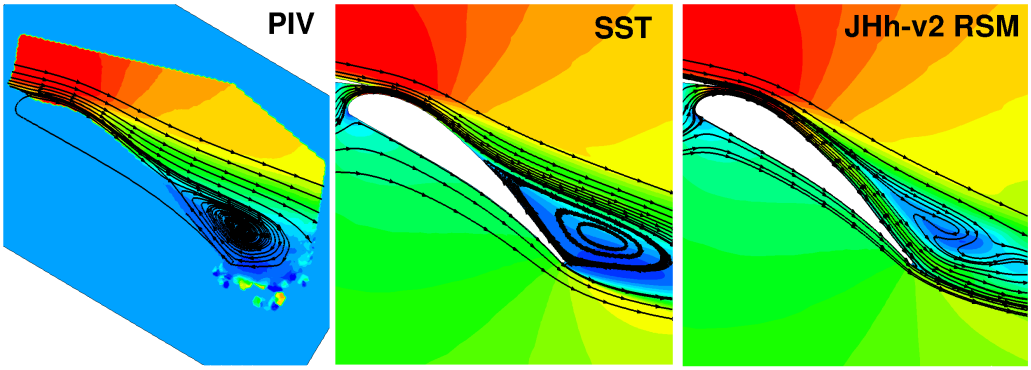

Figure 6: Mean-streamlines, averaged in time, from experiments and with the Menter-SST and JHh-v2 RSM model at $\alpha = 0°$ colored with the stream-wise velocity

In Fig. 6 the mean-streamlines, averaged in time, obtained in the PIV measurement, with the Menter-SST model and with the JHh-v2 RSM model are compared for the incidence angle of $\alpha = 0°$. The Menter-SST model predicts the separation on the flap in good agreement with the PIV data but the onset of the separation is predicted a little too early. The influence of the instability in the RSM simulation triggers some mechanism that prevents the flow from

separating at the flap. Instead an instability forms between the flow over the main wing and the flow through the gap between main wing and flap. This instability leaves a footprint in the mean-streamlines.

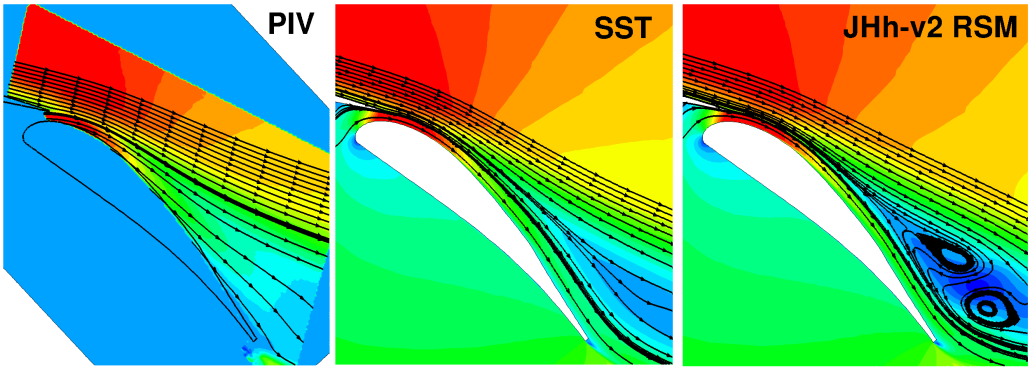

Figure 7: Mean-streamlines, averaged in time, from experiments and with the Menter-SST and JHh-v2 RSM model at $\alpha = 6°$ colored with the stream-wise velocity

The corresponding comparison for the $\alpha = 6°$ case is shown in Fig. 7. At this incidence angle the flow on the flap is attached. This behavior is predicted by both models but there is a general difference between experiment and simulations: In the experiment the flow through the gap thickens towards the trailing edge of the flap while no strong bending is observed in the streamlines of the flow over the main wing. In both simulations the streamlines from the main wing wake are bent towards the flap while the gap flow is parallel to the flap without much thickening. In the RSM results again an instability forms in the shear layer between the flow over the main wing and the gap flow which can also be seen in the time averaged streamlines.

4.2 Simulations with viscous wind tunnel walls

The most expensive approach in terms of computational resources is to include the whole measurement section in the numerical setup. Results from this approach predicted by the Menter-SST model and the JHh-v2 RSM model are shown in Fig. 8. Here, the skin-friction lines are compared with oil-flow pictures from the experiment at an angle of attack of $\alpha = 6°$.

In the upper row a view of the leading edge of the main wing from upstream is depicted and the lower row presents a view of the flap from downstream. The oil-flow visualization reveals a small separation region at the junction between main wing and side-wall. The flow is bent at the smooth transition region between the droop nose and the main profile but at a small distance towards the centerline section it is essentially undisturbed. The JHh-v2 RSM model that is shown in the center column predicts this separation region at the main wing in good agreement with the experimental observations. Opposed to that in the Menter-SST result the size of the separation is massively over-predicted. In the span-wise direction the flow is influenced by this separation over a great part of the main wing towards the centerline section.

The view of the flap shows again the large influence of the separation region in the SST simulation. The massively separated flow on the main wing shields the flow on the flap such that the separation at the junction between flap and wind tunnel wall is completely missing. Again the flow pattern is predicted much better by the RSM model even though the size of the separation at the junction between flap and tunnel wall is under-predicted.

Another observation in the three-dimensional Menter-SST simulation is an unphysical separation at the centerline section which is not in agreement with the PIV data. This seems to

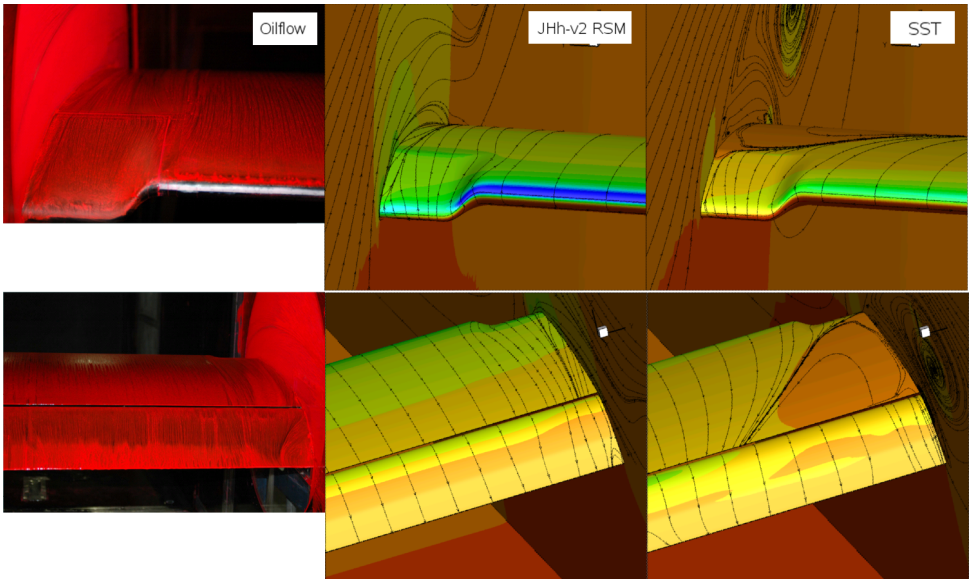

Figure 8: Oil-flow pictures and skin-friction lines from Menter-SST and JHh-v2 RSM model at $\alpha = 6°$

be due to the massively disturbed flow in the centerline section because of the over-predicted side-wall separation since in the two-dimensional simulations no separation was predicted at this incidence angle.

For the $\alpha = 0°$ case only Menter-SST results are available, so far. At this lower angle of attack, however, the SST model predicts the separation at the side wall reasonably well and the flow in the centerline direction is undisturbed by the side-wall separation. Also the size of the separation at the junction between the flap and the wind tunnel side-wall is predicted in good agreement with the oil-flow picture.

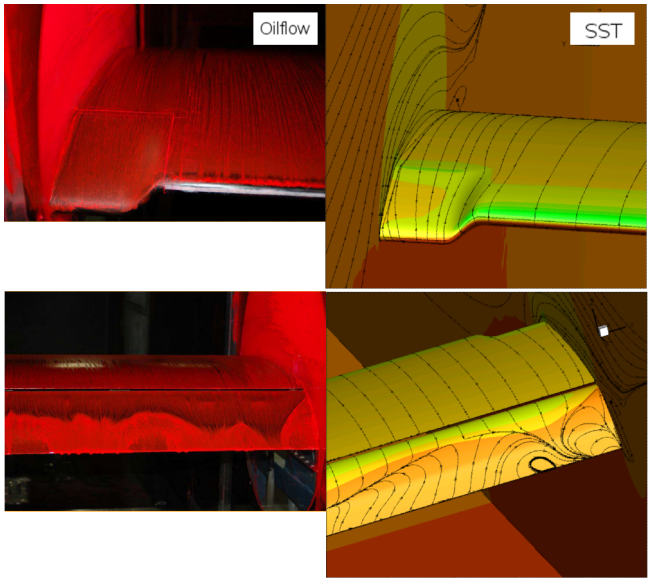

Figure 9: Oil-flow pictures and skin-friction lines from Menter-SST model at $\alpha = 0°$

The influences of the different approaches on the mean-pressure distribution in the centerline section of the wind tunnel can be seen in Fig. 10 for the angle of attack of $\alpha = 0°$.

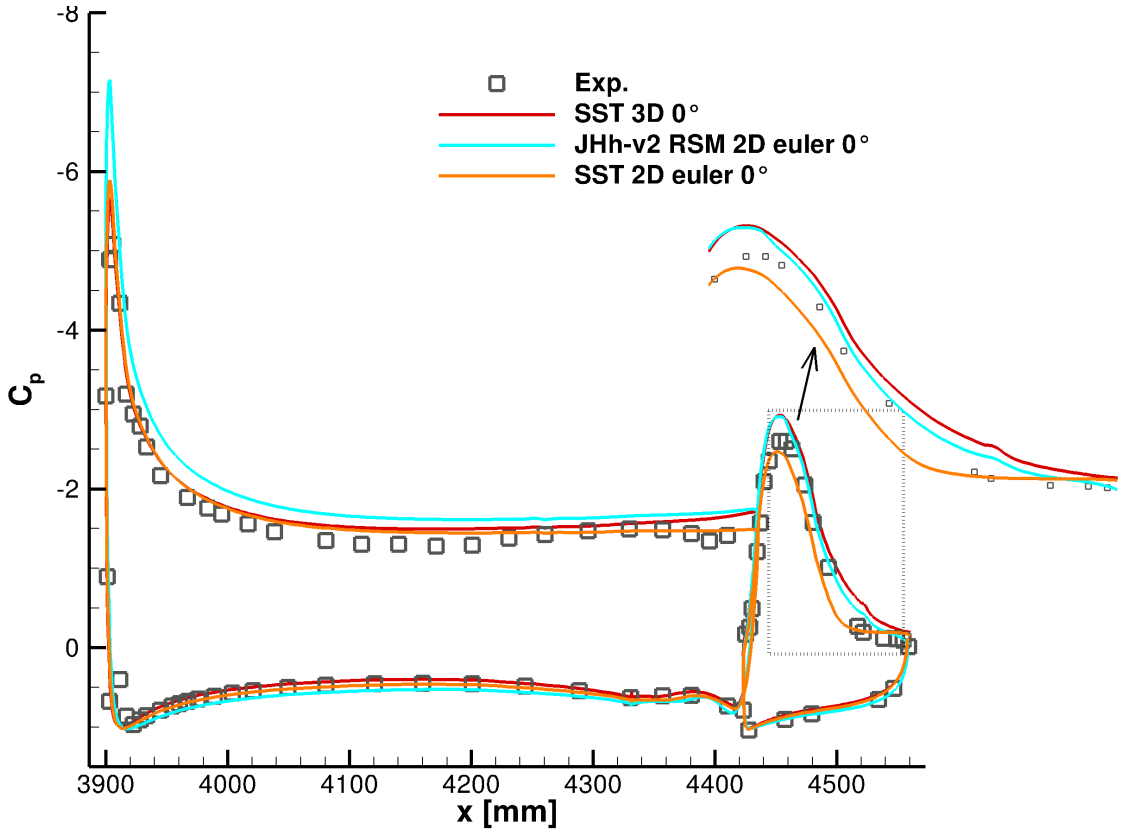

Figure 10: Comparison of the mean-pressure distribution obtained with different turbulence models and numerical setups at $\alpha = 0°$

For the two-dimensional Menter-SST simulation (orange line) the pressure distribution shows a plateau in the rear part of the flap as in the experimental data. Since the onset of the separation is to early as was shown in Fig. 6 the plateau builds too early and the suction peak is predicted too low. No such plateau can be seen in the two-dimensional JHh-v2 RSM simulation (light blue line) due to the attached flow on the flap. Therefore, the circulation is predicted wrong in the RSM simulation and the suction peaks are over-predicted on both elements and a larger offset from the experimental data can be observed at the main wing. The three-dimensional SST simulation (red line) predicts separation at the centerline section but the separation point is shifted downstream compared to the experimental data. In the mean-pressure distribution only a very small plateau can be seen close to the trailing edge of the flap. Therefore, the pressure distribution is much closer to the RSM on the flap. On the main wing however, the difference between the two- and three-dimensional SST simulations is very small. To further assess these results an additional three-dimensional simulation using the JHh-v2 RSM model is planned.

For the $\alpha = 6°$ case more simulations are compared in Fig. 11 and the outcome is more clear. Here, the third approach, the two-dimensional simulation with boundary layer resolution at the upper and lower wind tunnel wall, is included. For this approach the result from the Menter-SST model is presented.

The pressure distribution of the two-dimensional Menter-SST simulation with inviscid tunnel walls (orange line) is in very good agreement with the experimental data. The results that were obtained in the two-dimensional approach with boundary-layer resolution with the SST

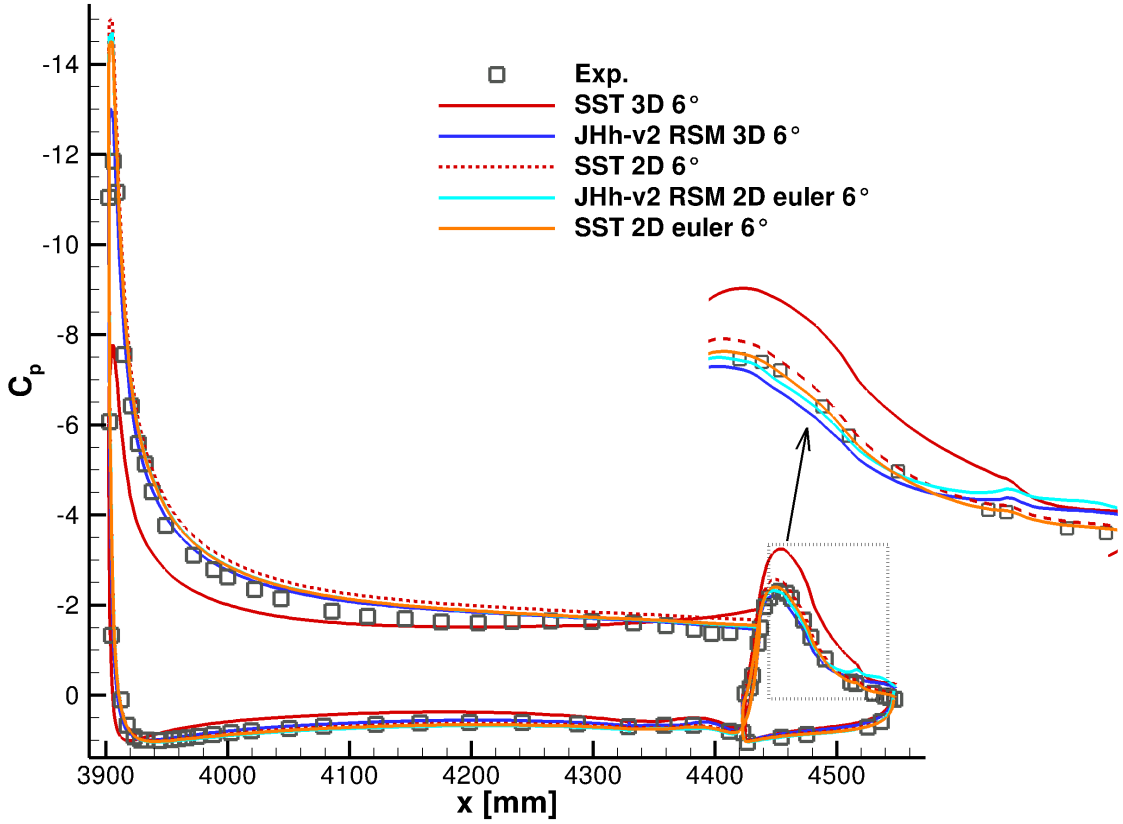

Figure 11: Comparison of the mean-pressure distribution obtained with different turbulence models and numerical setups at $\alpha = 6°$

model (dashed red line) show a little offset from the former results but the general behavior is not changed. Only the pressure distribution in the centerline section of the three-dimensional simulation using the Menter-SST model is completely different. This is due to the massive separation that is predicted at the side walls with this model.

The results from the two-dimensional JHh-v2 RSM simulation with inviscid tunnel walls (light blue line) almost coincide with the corresponding SST results on large parts of the profile. Only the instability above the flap leads to a bigger deviation from the experimental distribution for the RSM model. The pressure distribution in the centerline section of the three-dimensional simulation with the RSM model (blue line) is very close to the two-dimensional results.

5 Conclusion

Three different approaches to model the influence of the wind tunnel walls were compared. For the least expensive approach, neglecting the boundary layers at the tunnel walls and restricting the simulation to the centerline section of the wind tunnel, the grid resolution and time-step size were evaluated. Here, it was found that using the JHh-v2 RSM model leads to instabilities in the wing cove. A fast decay of the Reynolds-stresses behind the separation point was found to be responsible for this behavior.

In the three-dimensional simulation at an angle of attack of $\alpha = 6°$ the Menter-SST model predicted a massive separation of the flow at the junction between the profile and the wind tunnel wall that disturbed the flow even at the centerline section. However, for an angle of

attack of $\alpha = 0°$ the results with the Menter-SST model looked much better. The JHh-v2 RSM model was only applied for $\alpha = 6°$ and the flow at the model-tunnel junction was predicted in accordance with the experimental data.

Comparing the pressure distribution at an angle of attack of $\alpha = 6°$, the following could be observed: The influence of the boundary layer on the upper and lower wind tunnel wall in a two-dimensional simulation is very small. This could be shown for the Menter-SST model. The results using the JHh-v2 RSM model show good agreement between the centerline section of the three-dimensional simulation and the two-dimensional simulation with inviscid walls.

These results show that it is appropriate to neglect the influence of the wind tunnel walls in a simulation as long as the experiments are designed to minimize the side wall effects. The droop noses that were used in the present experiments are a good approach to achieve this goal in the case of multi-element airfoils.

In the future it is planned to apply turbulence resolving models to this test case. With respect to these simulation the current results are very important. Resolving the entire three-dimensional setup in a scale resolving approach is not feasible with the currently available computational resources. Based on this work it is now justified to restrict the computational domain to the centerline section of the wind tunnel.

Acknowledgments

The members of the FOR 1066 research group gratefully acknowledge the support of the "Deutsche Forschungsgemeinschaft DFG" (German Research Foundation) which funded this research.

References

[1] Cecora, R.-D., Eisfeld, B., Probst, A., Crippa, S., and Radespiel, R., "Differential Reynolds Stress Modeling for Aeronautics," AIAA Paper 2012-0465, January 2012.

[2] Hahn, D., Scholz, P. and Radespiel, R.: "Experimental evaluation of the stall characteristics of a two-element high-lift airfoil". Second Symposium "Simulation of Wing and Nacelle Stall" June 22nd - 23rd, Braunschweig, Germany, 2010.

[3] Schwamborn, D., Gerhold, T. and Heinrich, R.: "The DLR TAU-Code: recent applications in reaserach and industry". In "proceedings of ECCOMAS CFD 2006, Wesseling, P. Oñate, E. Périaux, J. (eds.), The Netherlands, TU Delft", 2006.

[4] Menter, F. R.: "Two-Equation Eddy-Viscosity Turbulence Models for Engineering Applications". AIAA Journal, Vol. 32, No. 8, pp. 1598-1605, August 1994.

[5] Jakirlić, S. and Hanjalić, K.: "A new approach to modelling near-wall turbulence energy and stress dissipation". Journal of Fluid Mechanics, 459:139–166, June 2002.